Dielectric function, screening, and plasmons in two-dimensional graphene

E. H. Hwang and S. Das Sarma
Condensed Matter Theory Center, Department of Physics, University of Maryland, College Park, Maryland 20742-4111, USA
(Received 4 October 2006; published 11 May 2007)

The dynamical dielectric function of two-dimensional graphene at arbitrary wave vector q and frequency ω, $\epsilon(q,\omega)$, is calculated in the self-consistent-field approximation. The results are used to find the dispersion of the plasmon mode and the electrostatic screening of the Coulomb interaction in two-dimensional (2D) graphene layer within the random-phase approximation. At long wavelengths ($q\rightarrow 0$), the plasmon dispersion shows the local classical behavior $\omega_{cl}=\omega_0\sqrt{q}$, but the density dependence of the plasma frequency ($\omega_0 \propto n^{1/4}$) is different from the usual 2D electron system ($\omega_0 \propto n^{1/2}$). The wave-vector-dependent plasmon dispersion and the static screening function show very different behavior than the usual 2D case. We show that the intrinsic interband contributions to static graphene screening can be effectively absorbed in a background dielectric constant.

DOI: 10.1103/PhysRevB.75.205418 PACS number(s): 73.21.−b, 71.10.−w, 73.43.Lp

I. INTRODUCTION

There has been a great deal of recent interest in the electronic properties of two-dimensional (2D) graphene, a single-layer graphite sheet, both theoretically and experimentally.[1,2] The main difference of 2D graphene compared with other (mostly semiconductor-based) 2D materials is the electronic energy dispersion. In conventional 2D systems, the electron energy with an effective mass m^* depends quadratically on the momentum, but in graphene, the dispersions of electron and hole bands are linear near K, K' points of the Brillouin zone. Because of the different energy band dispersions, screening properties in graphene exhibit significantly different behavior from the conventional 2D systems.[3] The screening of Coulomb interaction induced by many-body effects is one of the most important fundamental quantities for understanding many physical properties. For example, dynamical screening determines the elementary excitation spectra and the collective modes of the electron system, and static screening determines transport properties through screened Coulomb carrier scattering by charged impurities. In this paper, we theoretically obtain the (dynamical and static) screening behavior of 2D graphene by calculating the polarizability and the dielectric function within the self-consistent field approximation [i.e., random-phase approximation (RPA)] for gated-2D graphene free carrier systems. We apply our theory to calculate the 2D graphene plasmon dispersion and the static screening function, finding some interesting qualitative differences between graphene and the extensively studied 2D electron systems based on semiconductor heterostructures and metal-oxide-semiconductor field-effect transistors (MOSFETs).

In this paper, we calculate the dielectric function of graphene at arbitrary wave vector q and frequency ω, $\epsilon(q,\omega)$, within RPA, in which each electron is assumed to move in the self-consistent field arising from the external field plus the induced field of all electrons. This is the model which leads to the famous Lindhard dielectric function for a three-dimensional (3D) (Ref. 4) and 2D (Ref. 5) electron gas. One of the immediate theoretical consequences of the dielectric function is that its zeros give the wave-vector-dependent plasmon mode $\omega_{pl}(q)$, which is a fundamental elementary excitation and a collective density oscillation mode. Using the theoretical dielectric function, we provide the plasmon mode dispersion both for single-layer and bilayer graphene. Another important consequence of the dielectric function is the static screening function which can be obtained as the static limit $\omega\rightarrow 0$ of the dielectric function, describing the electrostatic screening of the electron-electron, electron-lattice, and electron-impurity interactions.

II. POLARIZABILITY: Π^+ AND Π^-

The electron dynamics in 2D graphene is modeled by a chiral Dirac equation, which describes a linear relation between energy and momentum. The corresponding kinetic energy of graphene for 2D wave vector $\mathbf{k}$ is given by (we use $\hbar=1$ throughout this paper)

$$\epsilon_{s\mathbf{k}} = s\gamma|\mathbf{k}|, \tag{1}$$

where $s=\pm 1$ indicate the conduction (+1) and valence (−1) bands, respectively, and γ is a band parameter (essentially, the 2D Fermi velocity, which is a constant for graphene instead of being density dependent). The corresponding density of states (DOS) is given by $D(\epsilon)=g_s g_v|\epsilon|/(2\pi\gamma^2)$, where $g_s=2$ and $g_v=2$ are the spin and valley degeneracies, respectively. The Fermi momentum (k_F) and the Fermi energy (E_F) of 2D graphene are given by $k_F=(4\pi n/g_s g_v)^{1/2}$ and $E_F=\gamma k_F$, where n is the 2D carrier (electron or hole) density. For the sake of completeness, we also mention that the dimensionless Wigner-Seitz radius (r_s), which measures the ratio of the potential to the kinetic energy in an interacting quantum Coulomb system,[4] is given in doped 2D graphene by $r_s=(e^2/\kappa\gamma)(4/g_s g_v)^{1/2}$, where κ is the background lattice dielectric constant of the system. We note in the passing the curious fact that the dimensionless r_s parameter is a *constant* in graphene unlike in the usual 2D ($r_s\sim n^{-1/2}$) and 3D ($r_s\sim n^{-1/3}$) electron liquids, where r_s (and, therefore, interaction effects) increases with decreasing carrier density. The constancy of r_s in graphene arises trivially from the relativistic Dirac-like nature of the free carrier graphene dynamics im-

plying that the "relativistic" effective mass, $m_c=E_F/\gamma^2$, depends on carrier density precisely as $\sqrt{n}$ canceling out the corresponding $\sqrt{n}$ term in the potential energy. Equivalently, r_s here is just the "effective fine structure constant" for graphene, with a value of $r_s\sim 0.5$, assuming $g_s=g_v=2$ and $\kappa=4$ (using SiO_2 as the substrate material). This small (and constant) value of graphene r_s indicates it to be a weakly interacting system for all carrier densities, making RPA an excellent approximation in graphene since RPA is asymptotically exact in the $r_s \ll 1$ limit.

In the RPA, the dynamical screening function (dielectric function) becomes

$$\varepsilon(q,\omega) = 1 + v_c(q)\Pi(q,\omega), \tag{2}$$

where $v_c(q)=2\pi e^2/\kappa q$ is the 2D Coulomb interaction, and $\Pi(q,\omega)$, the 2D polarizability, is given by the bare bubble diagram

$$\Pi(q,\omega) = -\frac{g_s g_v}{L^2}\sum_{\mathbf{k}ss'}\frac{f_{s\mathbf{k}}-f_{s'\mathbf{k}'}}{\omega+\epsilon_{s\mathbf{k}}-\epsilon_{s'\mathbf{k}'}+i\eta}F_{ss'}(\mathbf{k},\mathbf{k}'), \tag{3}$$

where $\mathbf{k}'=\mathbf{k}+\mathbf{q}$, $s,s'=\pm 1$ denote the band indices, and $F_{ss'}(\mathbf{k},\mathbf{k}')$ is the overlap of states and given by $F_{ss'}(\mathbf{k},\mathbf{k}')=(1+ss'\cos\theta)/2$, where θ is the angle between $\mathbf{k}$ and $\mathbf{k}'$, and f_{sk} is the Fermi distribution function, $f_{s\mathbf{k}}=[\exp\{\beta(\epsilon_{s\mathbf{k}}-\mu)\}+1]^{-1}$, with $\beta=1/k_BT$ and μ the chemical potential. After performing the summation over ss', we can rewrite the polarizability as

$$\Pi(q,\omega) = \Pi^+(q,\omega) + \Pi^-(q,\omega), \tag{4}$$

where

$$\Pi^+(q,\omega) = -\frac{g_s g_v}{2L^2}\sum_k\left[\frac{[f_{\mathbf{k}+}-f_{\mathbf{k}'+}](1+\cos\theta_{kk'})}{\omega+\epsilon_{\mathbf{k}+}-\epsilon_{\mathbf{k}'+}+i\eta} + \frac{f_{\mathbf{k}+}(1-\cos\theta_{kk'})}{\omega+\epsilon_{\mathbf{k}+}-\epsilon_{\mathbf{k}'-}+i\eta} - \frac{f_{\mathbf{k}'+}(1-\cos\theta_{kk'})}{\omega+\epsilon_{\mathbf{k}-}-\epsilon_{\mathbf{k}'+}+i\eta}\right] \tag{5}$$

and

$$\Pi^-(q,\omega) = -\frac{g_s g_v}{2L^2}\sum_k\left[\frac{[f_{\mathbf{k}-}-f_{\mathbf{k}'-}](1+\cos\theta_{kk'})}{\omega+\epsilon_{\mathbf{k}-}-\epsilon_{\mathbf{k}'-}+i\eta} + \frac{f_{\mathbf{k}-}(1-\cos\theta_{kk'})}{\omega+\epsilon_{\mathbf{k}-}-\epsilon_{\mathbf{k}'+}+i\eta} - \frac{f_{\mathbf{k}'-}(1-\cos\theta_{kk'})}{\omega+\epsilon_{\mathbf{k}+}-\epsilon_{\mathbf{k}'-}+i\eta}\right]. \tag{6}$$

For intrinsic (i.e., undoped or ungated with n and E_F both being zero) graphene, in which the conduction band is empty and the valence band is fully occupied at zero temperature (i.e., $E_F=0$), we have $f_{\mathbf{k}+}=0$ and $f_{\mathbf{k}-}=1$. Then the polarizability becomes $\Pi(q,\omega)=\Pi^-(q,\omega)$, which has been previously obtained in the renormalization group approach.[6] Recently, $\Pi^-(q,\omega)$ has been reconsidered to discuss screening effects of Coulomb interaction in intrinsic graphene.[7] In general, $\Pi^+(q,\omega)$ does not vanish for most systems because the Fermi energy is typically located in the conduction or the valence band. However, graphene is a most peculiar zero-gap semiconductor system, where $E_F=0$ in the intrinsic undoped situation. In the doped or gated situation n, $E_F\neq 0$ in graphene, and now Π^+ is finite. In the following, we provide the zero-temperature polarizability in the doped or gated case, where the Fermi energy is not zero.

By introducing the dimensionless quantities $x=q/k_F$ and $\nu=\omega/E_F$, and $\tilde{\Pi}(q,\omega)=\Pi(q,\omega)/D_0$, where $D_0\equiv D(E_F)=(g_s g_v n/\pi)^{1/2}/\gamma$ is the DOS at Fermi energy, we have

$$\tilde{\Pi}^+(x,\nu) = \tilde{\Pi}_1^+(x,\nu)\theta(\nu-x) + \tilde{\Pi}_2^+(x,\nu)\theta(x-\nu), \tag{7}$$

where the real parts of the polarizability are

$$\mathrm{Re}\,\tilde{\Pi}_1^+(x,\nu) = 1 - \frac{1}{8\sqrt{\nu^2-x^2}}\{f_1(x,\nu)\theta(|2+\nu|-x) + \mathrm{sgn}(\nu-2+x)f_1(x,-\nu)\theta(|2-\nu|-x) + f_2(x,\nu)[\theta(x+2-\nu)+\theta(2-x-\nu)]\}, \tag{8}$$

$$\mathrm{Re}\,\tilde{\Pi}_2^+(x,\nu) = 1 - \frac{1}{8\sqrt{x^2-\nu^2}}\left\{f_3(x,\nu)\theta(x-|\nu+2|) + f_3(x,-\nu)\theta(x-|\nu-2|) + \frac{\pi x^2}{2}[\theta(|\nu+2|-x) + \theta(|\nu-2|-x)]\right\}, \tag{9}$$

and the imaginary parts of the polarizability are

$$\mathrm{Im}\,\tilde{\Pi}_1^+(x,\nu) = \frac{-1}{8\sqrt{\nu^2-x^2}}\left\{f_3(x,-\nu)\theta(x-|\nu-2|) + \frac{\pi x^2}{2}[\theta(x+2-\nu)+\theta(2-x-\nu)]\right\}, \tag{10}$$

$$\mathrm{Im}\,\tilde{\Pi}_2^+(x,\nu) = \frac{\theta(\nu-x+2)}{8\sqrt{x^2-\nu^2}}[f_4(x,\nu) - f_4(x,-\nu)\theta(2-x-\nu)], \tag{11}$$

where

$$f_1(x,\nu) = (2+\nu)\sqrt{(2+\nu)^2-x^2} - x^2\ln\frac{\sqrt{(2+\nu)^2-x^2}+(2+\nu)}{|\sqrt{\nu^2-x^2}+\nu|}, \tag{12}$$

$$f_2(x,\nu) = x^2\ln\frac{\nu-\sqrt{\nu^2-x^2}}{x}, \tag{13}$$

$$f_3(x,\nu) = (2+\nu)\sqrt{x^2-(2+\nu)^2} + x^2\sin^{-1}\frac{2+\nu}{x}, \tag{14}$$

$$f_4(x,\nu) = (2+\nu)\sqrt{(2+\nu)^2 - x^2} - x^2 \ln \frac{\sqrt{(2+\nu)^2 - x^2} + (2+\nu)}{x}, \quad (15)$$

and $\tilde{\Pi}^-(x,\nu)$ can be calculated to be

$$\tilde{\Pi}^-(x,\nu) = \frac{\pi x^2 \theta(x-\nu)}{8\sqrt{x^2-\nu^2}} + i\frac{\pi x^2 \theta(\nu - x)}{8\sqrt{\nu^2 - x^2}}. \quad (16)$$

Equations (7)–(16) are the basic results obtained in this paper, giving the 2D-doped graphene polarizability analytically. Note that our 2D graphene polarizability is completely different from the corresponding 2D Lindhard function first calculated in Ref. 5 which is appropriate for the usual 2D systems with parabolic band dispersion.

III. PLASMONS IN RPA

As a significant consequence of the dielectric function, we calculate the long-wavelength plasmon dispersion for single-layer graphene and for bilayer graphene. The longitudinal collective-mode dispersion, or plasmon mode dispersion, can be calculated by looking for poles of the density correlation function, or equivalently, by looking for zeros of the dynamical dielectric function, $\epsilon(\mathbf{q},\omega) = 1 - v(q)\Pi(\mathbf{q},\omega)$. In the long-wavelength limit ($q \to 0$), we have the following limiting forms in the high- and low-frequency regimes:

$$\Pi(q,\omega) \approx \begin{cases} \dfrac{D_0 \gamma^2 q^2}{2\omega^2}[1 - (\omega^2/4E_F^2)], & \gamma q < \omega < 2E_F \\ D_0[1 + i(\omega/\gamma q)], & \omega < \gamma q. \end{cases} \quad (17)$$

In the $q \to 0$ limit, we have the plasmon mode dispersion $\omega_p(q)$ for a single-layer graphene as

$$\omega_{cl} \equiv \omega_p(q \to 0) = \omega_0 \sqrt{q}, \quad (18)$$

where $\omega_0 = (g_s g_v e^2 E_F/2\kappa)^{1/2}$. The leading order (or local) plasmon has exactly the same dispersion, $q^{1/2}$, as the normal 2D plasmon.[3] However, the density dependence of the plasma frequency in graphene shows a different behavior, i.e., $\omega_0 \propto n^{1/4}$ compared with the classical 2D plasmon behavior, where $\omega_0 \propto n^{1/2}$. This is a direct consequence of the quantum relativistic nature of graphene. Even though the long-wavelength plasmons have identical dispersions for both cases, the dispersion calculated within RPA including finite-wave-vector nonlocal (i.e., higher order in q) effects shows very different behavior. In normal 2D,[3,5] the nonlocal correction leads to an increase in plasma frequency, $[\omega_p(q)/\omega_{cl} = 1 + (3/4)(q/q_{TF})]$, where $q_{TF} = g_s g_v m e^2/\kappa$ is the usual 2D Thomas-Fermi wave vector, but in graphene the correction within RPA leads to a decrease in plasma frequency compared with ω_{cl} $[\omega_p(q)/\omega_{cl} = 1 - q_0 q/8k_F^2]$, where $q_0 = g_s g_v e^2 k_F/\gamma\kappa$ is the corresponding graphene Thomas-Fermi wave vector. Recently, the plasmon mode of graphene has been considered numerically in the presence of spin-orbit coupling.[8]

For bilayer graphene, *without interlayer hopping*, we have the leading order q dependence of the collective modes by solving a two component determinantal equation,[9,10]

$$\omega_+(q) \approx \omega_0 \sqrt{2q},$$

$$\omega_-(q) \approx 2\omega_0 \sqrt{dq}, \quad (19)$$

where d is the layer separation between the two 2D graphene sheets. The ω_+ mode, the optical-plasmon mode (in-phase mode of the coupled system), has the well-known $q^{1/2}$ behavior, independent of the layer separation d at long wavelengths. The other mode ω_- is the acoustic plasmon mode (out-of-phase mode of the coupled system), which goes as q in long wavelengths and depends on the separation d. Thus, the coupled plasmons in graphene show the same long-wavelength behaviors as those of normal 2D systems. However, the density dependences of the plasma frequency and the large wave-vector dependences are again very different from the corresponding normal 2D systems.[9] When interlayer hopping is included in a bilayer system, the in-phase plasmon mode is qualitatively unaffected by tunneling. However, the out-of-phase plasmon mode develops a long-wavelength gap (depolarization shift) in the presence of tunneling,[14] i.e., $\omega_-(q \to 0) = (2t_\perp)^2(1 + q_0 d)$, where $t_\perp$ is the interlayer hopping. Due to strong interlayer coupling in bilayer graphene, in general, we have $\omega_+ \ll \omega_-$ at long wavelengths.

In Fig. 1, we show the calculated plasmon dispersion within RPA (solid line) compared with the classical local plasmon (dashed line). We use the following parameters: $\kappa = 2.5$, $\gamma = 6.5$ eV Å, and a density $n = 10^{12}$ cm^{-2}. In Fig. 1(b), we show the corresponding 2D regular plasmons with n-GaAs parameters ($n = 5 \times 10^{11}$ cm^{-2}). In Fig. 1, we also show the electron-hole continuum or single-particle excitation (SPE) region in (q,ω) space, which determines the absorption (Landau damping) of the external field at given frequency and wave vector. The SPE continuum is defined by the nonzero value of the imaginary part of the polarizability function, $\mathrm{Im}\,\Pi(q,\omega) \neq 0$. For a normal 2D system, only indirect ($q \neq 0$) transition is possible within the band, and the SPE boundaries are given by $\omega_{1,2} = q^2/2m \pm q k_F/m$. However, for 2D graphene, both intraband and interband transitions are possible, and the boundaries are given in Fig. 1(a). The intraband SPE boundaries are $\omega_1 = \gamma q$ (upper boundary) and $\omega_2 = 0$ for $q < 2k_F$, $\omega_2 = \gamma q - 2E_F$ for $q > 2k_F$ (lower boundary). The direct transition ($q = 0$) is also possible from the valence band to the empty conduction band. Due to the phase-space restriction, the interband SPE continuum has a gap at small wave vectors. For $q = 0$, the transition is not allowed at $0 < \omega < 2E_F$. If the collective mode lies inside the SPE continuum, we expect the mode to be damped. Since the normal 2D plasmon lies, at long wavelengths, above the SPE continuum, it never decays to electron-hole pair within RPA. However, for graphene, the plasmon lies inside the interband SPE continuum decaying into electron-hole pairs. Only in the region I of Fig. 1(a) the plasmon is not damped. The other different feature between a normal 2D plasmon and a graphene plasmon occurs at large wave vectors. The normal 2D plasmon mode enters into the SPE continuum at a critical

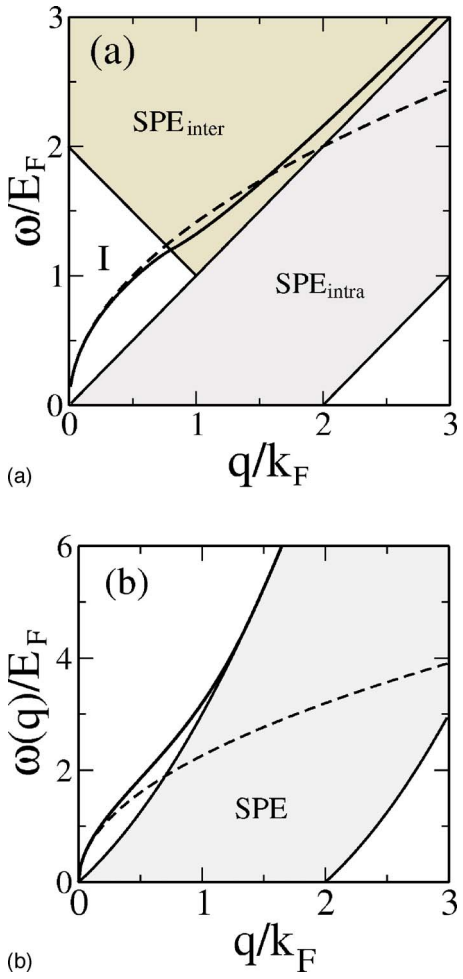

FIG. 1. (Color online) (a) Plasmon mode dispersion in 2D graphene (solid thick line) calculated within RPA. The dashed line indicates the local long-wavelength plasmon dispersion. Thin solid lines represent the boundaries of the single-particle excitation (SPE) Landau damping regime for intra- and interband electron-hole excitations. (b) The plasmon dispersion and SPE for a normal 2D system with a quadratic energy dispersion.

wave vector, and, therefore, does not exist at very high wave vectors. All spectral weight of the plasmon mode is transferred to the SPE. However, the graphene plasmon does not enter into the intraband SPE and exists for all wave vectors, except for its decay into real interband electron-hole pairs in theSPE$_{\text{inter}}$ regime.

IV. STATIC SCREENING

Now we consider the static polarizability $\Pi(q,\omega=0)$. From Eq. (9), we have

$$\tilde{\Pi}^{+}(q) = \begin{cases} 1 - \dfrac{\pi q}{8k_F}, & q \le 2k_F \\ 1 - \dfrac{1}{2}\sqrt{1 - \dfrac{4k_F^2}{q^2}} - \dfrac{q}{4k_F}\sin^{-1}\dfrac{2k_F}{q}, & q > 2k_F, \end{cases} \tag{20}$$

and from Eq. (16), we have

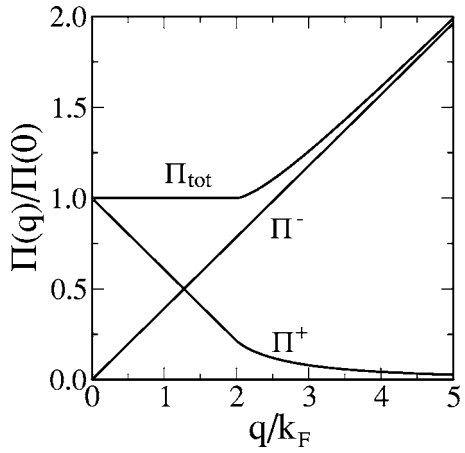

FIG. 2. Static polarizability for 2D graphene: $\Pi_{tot}=\Pi^{+}+\Pi^{-}$. Here $\Pi(0)=D(E_F)=g_s g_v k_F/2\pi\gamma$.

$$\tilde{\Pi}^{-}(q) = \pi q/8k_F. \tag{21}$$

Thus, the total static polarizability becomes a constant at $q \le 2k_F$ as in a normal 2D systems, i.e., $\Pi(q)=\Pi^{+}(q)+\Pi^{-}(q) = D(E_F)$ for $q \le 2k_F$. In Fig. 2, we show the calculated static polarizability as a function of wave vector. For a normal 2D system, the screening wave vector, $q_s=q_{TF}=g_s g_v me^2/\kappa$, is independent of electron concentration, but for 2D graphene, the screening wave vector is given by $q_s=g_s g_v e^2 k_F/\kappa\gamma$, which is proportional to the square root of the density, $n^{1/2}$. In the large momentum transfer regime, $q > 2k_F$, the static screening increases linearly with q due to the interband transition. This is a very different behavior from a normal 2D system where the static polarizability falls off rapidly for $q > 2k_F$ with a cusp at $q=2k_F$.[3] The linear increase of the static polarizability with q gives rise to an enhancement of the effective dielectric constant $\kappa^{*}(q\to\infty)=\kappa(1+g_s g_v \pi r_s/8)$ in graphene. Note that in a normal 2D system, $\kappa^{*}\to\kappa$ as $q\to\infty$. Thus, the effective interaction in 2D graphene decreases at short wavelengths due to polarization effects. This large wave-vector screening behavior is typical of an insulator. Thus, 2D graphene screening is a combination of "metallic" screening (due to Π^{+}) and "insulating" screening (due to Π^{-}), leading to overall rather strange screening properties, all of which can be traced back to the zero-gap chiral relativistic nature of graphene.

In may be worthwhile to ask whether the *intrinsic* graphene contribution, arising strictly from the interband transitions due to the filled valence band (i.e., the Π^{-} term in our graphene polarizability), can be absorbed in the effective background lattice dielectric constant κ, just as one does in a regular semiconductor ($\kappa_{\text{Si}}=11.5$; $\kappa_{\text{GaAs}}=12.9$) or insulator ($\kappa_{\text{SiO}_2}=3.9$) in discussing free carrier screening by doping or gating, indeed, free carriers in conduction (electrons) or valence (holes) bands. In particular, only *intraband* free carrier screening is explicitly considered in the usual 2D screening function[3,5] extensively used[13,14] in the quantitative analysis of quantum transport in 2D semiconductor devices, such as Si MOSFETs, GaAs modulation-doped high-mobility transistors, and undoped gated GaAs heterostructures. The inter-

band transition induced screening in the semiconductor-based 2D structures is included in the theory simply by appropriately modifying the effective background lattice dielectric constant from the usual vacuum value of unity to a value around 10.

To see whether the effect of the interband Π^- polarizability can be "trivially" absorbed in a background lattice dielectric constant, we rewrite a 2D graphene dielectric function $\epsilon(q)=1+v_c(q)\Pi(q)$ to obtain

$$\epsilon(q) = 1 + \frac{2\pi e^2}{\kappa q}[\Pi^-(q) + \Pi^+(q)]. \tag{22}$$

Using Eq. (21), $\Pi^-(q)=D(E_F)\pi q/8k_F$, we get $v_c(q)\Pi^-(q) = \frac{g_s g_v \pi}{8}\frac{e^2}{\kappa\gamma} = \frac{g_s g_v \pi}{8} r_s$. Thus, we have

$$\epsilon(q) = 1 + \frac{g_s g_v \pi}{8} r_s + v_c(q)\Pi^+(q). \tag{23}$$

Introducing an effective intrinsic background graphene dielectric constant

$$\kappa^* = 1 + g_s g_v \pi r_s/8, \tag{24}$$

we have

$$\epsilon(q) = \kappa^*\left[1 + \frac{2\pi e^2}{\kappa\kappa^* q}\Pi^+(q)\right]. \tag{25}$$

Writing an effective *free carrier* 2D graphene dielectric function

$$\epsilon^+(q) \equiv 1 + v_c^+(q)\Pi^+(q), \tag{26}$$

where $v_c^+(q)=2\pi e^2/\kappa\kappa^* q$, we have

$$\epsilon(q) \equiv \kappa^* \epsilon^+(q). \tag{27}$$

Equation (27) shows that the intrinsic screening contribution arising from the interband Π^- term can be completely subsumed by introducing an effective graphene background lattice dielectric constant $\kappa^*=1+g_s g_v \pi r_s/8$, and by making the replacement $\kappa \to \kappa\kappa^*$ throughout. Introducing the effective dielectric constant κ^* allows one to use only the free carrier screening function,

$$\epsilon^+(q) = 1 + \frac{2\pi e^2}{\kappa\kappa^* q}\Pi^+(q), \tag{28}$$

for describing free carrier screening properties of 2D graphene. We note that κ itself here is the background lattice dielectric constant arising from the insulating substrate (i.e., SiO_2 in most situations) with $\kappa=(1+\kappa_{SiO_2})/2\approx 2.5$, and $\kappa^* = 1+g_s g_v \pi r_s/8 \approx 2.3$ with $r_s=e^2/\kappa\hbar\gamma\approx 0.7$ for graphene on SiO_2 substrate. Thus, the substitution $\kappa\to\kappa\kappa^*$, arising from the interband contributions, enhances the effective background graphene dielectric constant to $\kappa\kappa^*\approx 6$—this approximate factor of 2 increase in the background dielectric constant arising from interband contributions further suppresses Coulomb interaction effects in extrinsic graphene.

The large q behavior of graphene dielectric screening, $\epsilon(q\to\infty)\to\kappa^*=1+g_s g_v \pi r_s/8$, again demonstrates that the short-wavelength screened Coulomb potential in 2D graphene goes as $2\pi e^2/\kappa\kappa^* q$, with an enhanced background effective dielectric constant $\kappa\kappa^*$, where κ is the effective background dielectric constant arising from the substrate and κ^* arising from graphene interband polarizability Π^- as discussed above. This implies that a suspended 2D graphene film, without any substrate (i.e., $\kappa=1$), would have an effective background lattice dielectric constant of $\kappa^*=1+g_s g_v \pi r_s/8$ with $r_s=e^2/\hbar\gamma$ (since $\kappa=1$). Putting in $g_s g_v=4$, we get $\kappa^*\approx 4$. Thus, the background static lattice dielectric constant of intrinsic graphene, due to interband transitions, is around 4.

If the $T=0$ transport properties of graphene are dominated by charged impurity scattering, as is thought to be the case,[15] then the long-wavelength Thomas-Fermi screening becomes an important input for calculating the screened charged impurity potential: $\epsilon_{TF}(q)\equiv\epsilon_{RPA}(q\to 0)$ becomes

$$\epsilon_{TF}(q) = 1 + q_{TF}/q, \tag{29}$$

where $q_{TF}\equiv q_s = g_s g_v e^2 k_F/\kappa\gamma$. Note that one can equivalently define a long-wavelength effective TF screening function $\epsilon_{TF}^+(q)$, where interband screening effects are absorbed in an effective background dielectric constant κ^*;

$$\epsilon_{TF}^+(q) = 1 + q_{TF}^*/q, \tag{30}$$

where $q_{TF}^*=q_{TF}/\kappa^*$. As discussed above, the identity, $\epsilon(q) \equiv \kappa^*\epsilon^+(q)$, guarantees the equivalence between Eqs. (29) and (30) for long-wavelength graphene screening. We note also that the $q=0$ screening wave vector q_{TF} is simply proportional to the graphene density of states at the Fermi level at $T=0$.

Although the two screening descriptions, based on $\epsilon(q)$ with the background dielectric constant being just κ and on $\epsilon^+(q)$ with the background dielectric constant being $\kappa\kappa^*$, are precisely equivalent for $T=0$ static screening properties, the two descriptions are *not* inequivalent at finite temperatures. Therefore, it is more appropriate to use the full dielectric function $\epsilon(q)$ in theoretical work on 2D graphene.

V. CONCLUSION

In conclusion, we have theoretically obtained analytic expressions for doped (i.e., $E_F\neq 0$) 2D extrinsic graphene polarizability, dielectric function, plasmon dispersion, and static screening properties, finding a number of intriguing qualitative differences with the corresponding normal (and extensively studied) 2D electron systems. The differences, with interesting observable consequences, can all be understood as arising from the zero-band gap intrinsic nature of undoped graphene with chiral linear relativistic bare carrier energy band dispersion. Some of our qualitatively predictions, such as the $n^{1/4}$ dependence of the long-wavelength graphene plasma frequency in contrast to the well-known $n^{1/2}$ behavior of classical and normal 2D plasmons, should be easily verifiable experimentally using the standard experimental techniques of infrared absorption[11] and/or inelastic light scattering[12] spectroscopies. Similarly, our prediction of the peculiar nature of the graphene plasmon damping (i.e., *no* Landau damping due to intraband electron-hole pairs, but finite Landau damping due to interband electron-hole pairs)

should be easily verifiable. Our predicted different screening behavior in graphene at large wave vector should have consequences for transport properties. Our RPA theory should be an excellent qualitative approximation for 2D graphene properties at all carrier densities (as long as the system remains a *homogeneous* 2D carrier system, which may not be true for $n \lesssim 10^{12}$ cm^{-2}), since the effective r_s parameter for graphene is a constant (<1), making RPA quantitatively accurate in graphene. Finally, we point out that the effective Fermi temperature, $T_F = E_F/k_B$, being very high (~ 1300 K for $n \sim 10^{12}$ cm^{-2}) in graphene; our $T=0$ theory should apply all the way to room temperatures. We note that the long-wavelength dielectric function for bulk graphite was earlier considered within an approximation scheme in Ref. 16 and the zero-frequency limit was recently considered in Ref. 17

Before concluding, we point out that some aspects of graphene collective modes and linear response have been discussed in the recent literature. In particular, the intrinsic situation without any free carriers has been considered in Ref. 7, whereas our emphasis in this work has been *extrinsic* graphene with free carriers (electrons and/or holes in conduction and/or valence band) induced by external gating or doping. There has been a recent purely numerical study[8] of graphene collective-mode spectra in the presence of spin-orbit coupling.

Note added. Recently, we became aware of related work.[18]

ACKNOWLEDGMENTS

This work is supported by the US-ONR, the LPS, and the Microsoft corporation.

[1] K. S. Novoselov, A. K. Geim, S. V. Morozov, D. Jiang, M. I. Katsnelson, I. V. Grigorieva, S. V. Dubonos, and A. A. Firsov, Nature (London) **438**, 197 (2005); Science **306**, 666 (2004).
[2] Y. Zhang, Y. W. Tan, H. L. Stormer, and P. Kim, Nature (London) **438**, 201 (2005).
[3] T. Ando, A. B. Fowler, and F. Stern, Rev. Mod. Phys. **54**, 437 (1982).
[4] G. D. Mahan, *Many Particle Physics* (Plenum, New York, 1993).
[5] Frank Stern, Phys. Rev. Lett. **18**, 546 (1967).
[6] J. Gonzalez, F. Guinea, and M. A. H. Vozmediano, Nucl. Phys. **424**, 595 (1994).
[7] D. V. Khveshchenko, Phys. Rev. B **74**, 161402(R) (2006); O. Vafek, Phys. Rev. Lett. **97**, 266406 (2006).
[8] X. F. Wang and T. Chakraborty, Phys. Rev. B **75**, 033408 (2007); **75**, 041404(R) (2007).
[9] S. Das Sarma and A. Madhukar, Phys. Rev. B **23**, 805 (1981).
[10] S. Das Sarma and E. H. Hwang, Phys. Rev. Lett. **81**, 4216 (1998).
[11] S. J. Allen, Jr., D. C. Tsui, and R. A. Logan, Phys. Rev. Lett. **38**, 980 (1977).
[12] D. Olego, A. Pinczuk, A. C. Gossard, and W. Wiegmann, Phys. Rev. B **25**, 7867 (1982).
[13] F. Stern, Phys. Rev. Lett. **44**, 1469 (1980).
[14] S. Das Sarma and E. H. Hwang, Phys. Rev. Lett. **83**, 164 (1999); Solid State Commun. **135**, 579 (2005); Phys. Rev. B **69**, 195305 (2004).
[15] E. H. Hwang, S. Adam, and S. Das Sarma, Phys. Rev. Lett. **98**, 186806 (2007).
[16] Kenneth W.-K. Shung, Phys. Rev. B **34**, 979 (1986).
[17] T. Ando, J. Phys. Soc. Jpn. **75**, 074716 (2006).
[18] B. Wunsch, T. Stauber, F. Sols, and F. Guinea, New J. Phys. **8**, 318 (2006).